

FINAL TECHNICAL REPORT

Regionalized Crustal Attenuation Tomography for the Continental US Using Higher-Order Ambient-Field Correlation

Gregory C. Beroza and Xin Liu

STANFORD UNIVERSITY

DEPARTMENT OF GEOPHYSICS

397 Panama Mall

Stanford, CA, 94305-2215

Telephone: (650)723-4746; fax: (650) 725-7344

Principal Investigator: Gregory C. Beroza (beroza@stanford.edu)

Keywords: Attenuation, USArray

Program Element III: U. S. Geological Survey National Earthquake Hazards Reduction Program Award
Number G18AP00046

Project Period: 7/2018-6/2019

Research supported by the U.S. Geological Survey (USGS), Department of the Interior, under USGS award number G18AP00046. The views and conclusions contained in this document are those of the authors and should not be interpreted as necessarily representing the official policies, either expressed or implied, of the U.S. Government

Abstract

Seismic wave attenuation provides important additional information to elastic structure for the shallow subsurface because it is sensitive to fractures, temperature, composition, and fluid content. It also has an important influence on earthquake strong ground motion. We develop a method based on noise cross-correlations of linear triplet of stations [Liu et al., 2015] that measures the relative amplitude decay of the ambient seismic field. We assume that the quality factor, Q , is constant, and that the ratios of site amplification factors are constant for different frequencies within each narrow band. We apply this technique to the amplitude measurements from USArray noise interferometry, and find reasonable correlations for the inverted attenuation $1/Q$ values between both the causal and anticausal parts of noise cross-correlations. The USArray attenuation tomography maps at different periods correspond to geological/tectonic features, including Yellowstone, the Colorado Plateau and others. Smoothed versions of the map show the well-known distribution of stronger attenuation in the western US than in the central and eastern US, and provide a potential approach to carry out quantitative Q regionalization even in areas that lack seismicity.

1 Introduction

Seismic wave attenuation provides complementary information to seismic velocity structure. The seismic attenuation quality factor Q is proportional to the seismic wave energy E divided by the energy loss per cycle ΔE : $Q = 2\pi E/\Delta E$.

Prieto et al. [2009] introduced a new empirical method for estimate the attenuation by fitting the cross-coherence of ambient noise to a Bessel function scaled by an exponential decay term with distance. Lawrence and Prieto [2011] used this method to estimate attenuation in the western US. Bowden et al. [2017] independently solved for the attenuation and site amplification from the Helmholtz equation by taking spatial gradients and Laplacians.

In this report, we invert for attenuation using linear triplets of stations within north-south lines of US-Array.

2 Data and methodology

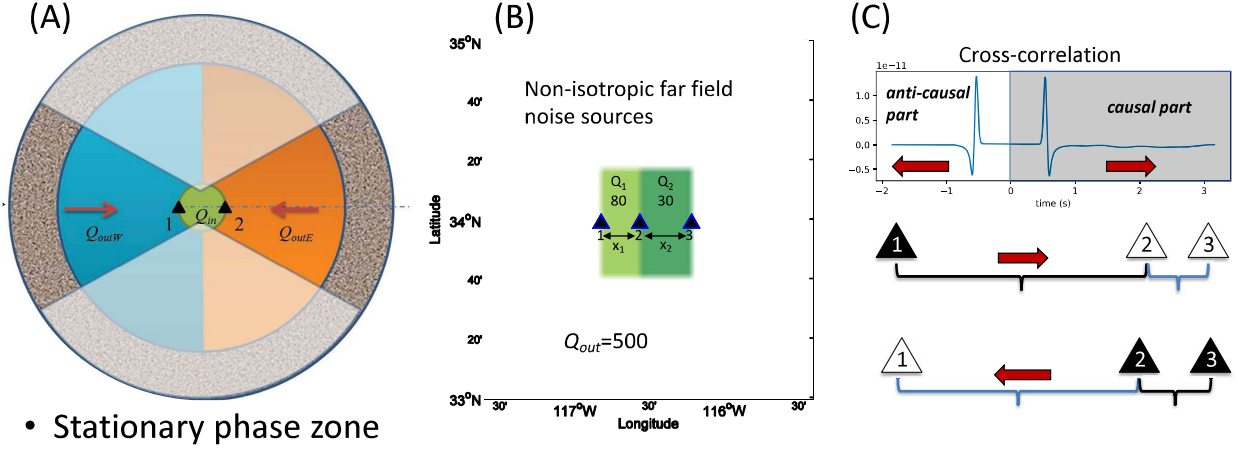


Figure 1: Illustrations of the attenuation inversion method. A) Seismic noise interferometry between two stations. The sectors along-strike show the stationary phase zone in which the noise sources' contributions stack constructively. B) The geometry for attenuation inversion using linear triplet of stations. C) Two combinations of triplet stations: causal (diverging) and anticausal (converging) amplitudes.

We downloaded the USArray data from IRIS DMC website (<https://ds.iris.edu/ds/nodes/dmc/>). The transportable array (TA) seismometers were rolled out across the continental US between 2005 and 2015, from the west coast to the east coast.

We process the ambient noise recordings for noise interferometry based on [Liu et al., 2016]. We cross correlate the noise recordings from the vertical components (Z) of the stations within each north-south line. We use evenly spaced time windows with 625 s window length and 125 sec gap to compute cross-correlations among different stations within each line. Earthquake and other transient signals are removed statistically from the continuous noise data following Liu et al. [2016]. Because of the rolling fashion of USArray, we stack exactly the same days of noise cross-correlations for each line in the USArray to ensure that the attenuation

estimations for all station pairs within the line are not affected by temporal variations of noise sources. The different data availability leads to varying Signal-Noise Ratio (SNR) for different numbers of stacked days for different lines in USArray.

The attenuation inversion method is based on the surface wave amplitude ratios between station pairs among a linear triplet of stations [Liu et al., 2015]. For seismic noise interferometry between two receivers, the ambient noise recordings from noise sources within the stationary phase zone (Fresnel zone) interfere constructively (Fig. 1A). To reduce the effect of noise sources, we compute the amplitude ratios from two pairs of stations within a linear triplet of stations (Fig. 1B) and fit the logarithmic amplitude ratios to a linear regression model for $1/Q$ values. We sequentially choose each station in the line as the virtual source and cross-correlate its noise data with other stations in the same line. The causal parts of the correlations represent the waves diverging the virtual source while the anticausal parts represent waves emitted by other stations converging to the virtual source. As an example using both the causal and anticausal parts of noise cross-correlation, we show three stations on a line and the distance between stations 2 & 3 is much smaller than that between stations 1 & 2 (Fig. 1C). For the causal parts of noise cross-correlations, the $1/Q$ value can be estimated by a simple linear least-squares equation [Liu et al., 2015],

$$\ln \tilde{C}_{13}^+(\omega) - \ln \tilde{C}_{12}^+(\omega) = \frac{-\omega \Delta t_{23}}{2Q_{23}^+} + \ln \frac{\gamma_3}{\gamma_2}, \quad (1)$$

where \tilde{C}_{13}^+ and \tilde{C}_{12}^+ are causal part amplitudes for the pairs 1-3 and 1-2, respectively, after correction for geometrical spreading. The ratio of site amplification factors γ_3 and γ_2 is assumed constant in a narrow frequency band. The travel time difference between stations 2 & 3 is $\Delta t_{23} = t_{13} - t_{12}$. The natural logarithm is $\ln(\cdot)$.

For the anticausal parts of noise cross-correlation, a similar linear least-square equation can be formulated to estimate the attenuation between stations 2 & 3,

$$\ln \tilde{C}_{13}^-(\omega) - \ln \tilde{C}_{12}^-(\omega) = \frac{-\omega \Delta t_{23}}{2Q_{23}^-} + \ln \frac{\gamma_3}{\gamma_2} \quad (2)$$

where \tilde{C}_{13}^- and \tilde{C}_{12}^- are anticausal part amplitudes for the pairs 1-3 and 1-2, respectively, after correction for geometrical spreading.

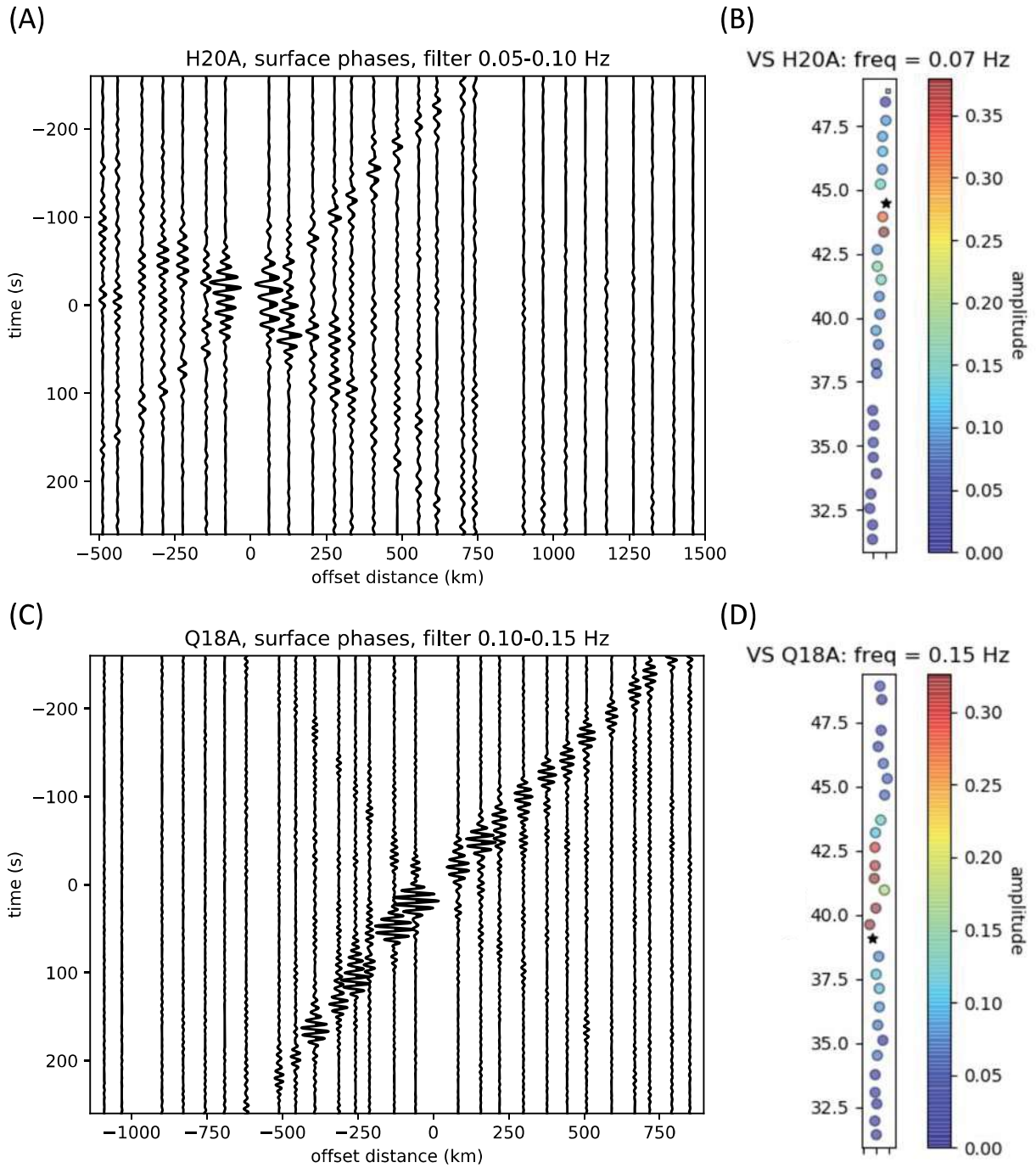


Figure 2: Examples of amplitude measurements from USArray lines. A) The noise cross-correlations filtered between 0.05-0.10 Hz for the virtual source H20A in line 20. B) The causal part amplitude measurements for panel A. C) The noise cross-correlations filtered between 0.10-0.15 Hz for the virtual source Q18A in line 18. D) The causal part amplitude measurements for panel C.

For the virtual source H20A in line 20, we plot its vertical cross-correlations filtered between 0.05-0.10 Hz with all other stations in the same line (Fig. 2A). The corresponding causal part ($time > 0$) amplitude measurements are shown in Fig. 2B. The gradually decaying amplitude on both sides of the virtual source is evident that attenuation and geometrical spreading damp the amplitude. For the virtual source Q18A in line 18, the noise cross-correlations bandpass filtered between 0.10-0.15 Hz are plotted in Fig. 2C with more asymmetry than those filtered by a lower frequency band 0.05-0.10 Hz. We observe the general trend of decaying amplitude for both North and South traveling waves from the causal part amplitude measurements at 0.15 Hz (Fig. 2D). Several obvious outliers are possibly related to abrupt changes in site amplifications and are removed in subsequent attenuation inversion.

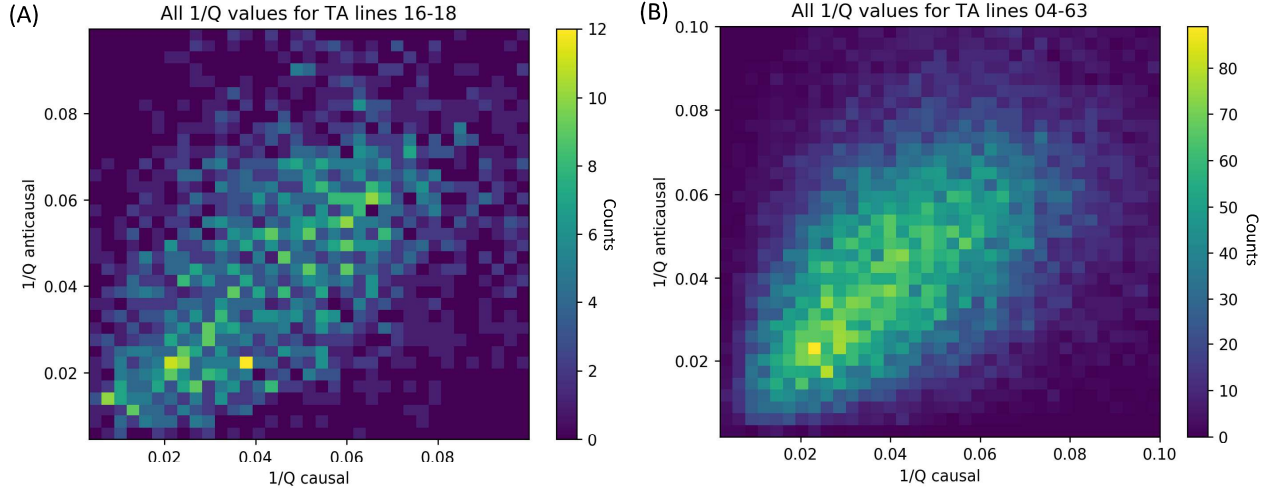


Figure 3: Statistics between the causal and anticausal attenuation $1/Q$ measurements for A) USArray lines 16-18 and B) USArray lines 4-63. The histogram represents number of measurements (scattered data points) in each grid cell.

We compute the $1/Q$ values from all inline triplets of stations for all lines in USArray with at least 30 days of common noise data within each line. For lines 16-18 covering the Yellowstone caldera, the $1/Q$ values derived from causal and anticausal parts of noise cross-correlations are shown in a density scatter plot (Fig. 3A) with a correlation coefficient of 0.468. The highest density values appear near the central line where the causal and anticausal $1/Q$ values are equal. Using the inverted $1/Q$ values from all USArray lines between 4 & 63, we again show the density scatter plot between the causal and anticausal $1/Q$ values (Fig. 3B) with a correlation coefficient of 0.421. These two examples indicate that, despite the asymmetry in noise cross-correlation and varying SNR, the attenuation $1/Q$ derived from the causal and anticausal amplitudes are correlated to a reasonable extent.

3 Attenuation regionalization using USArray

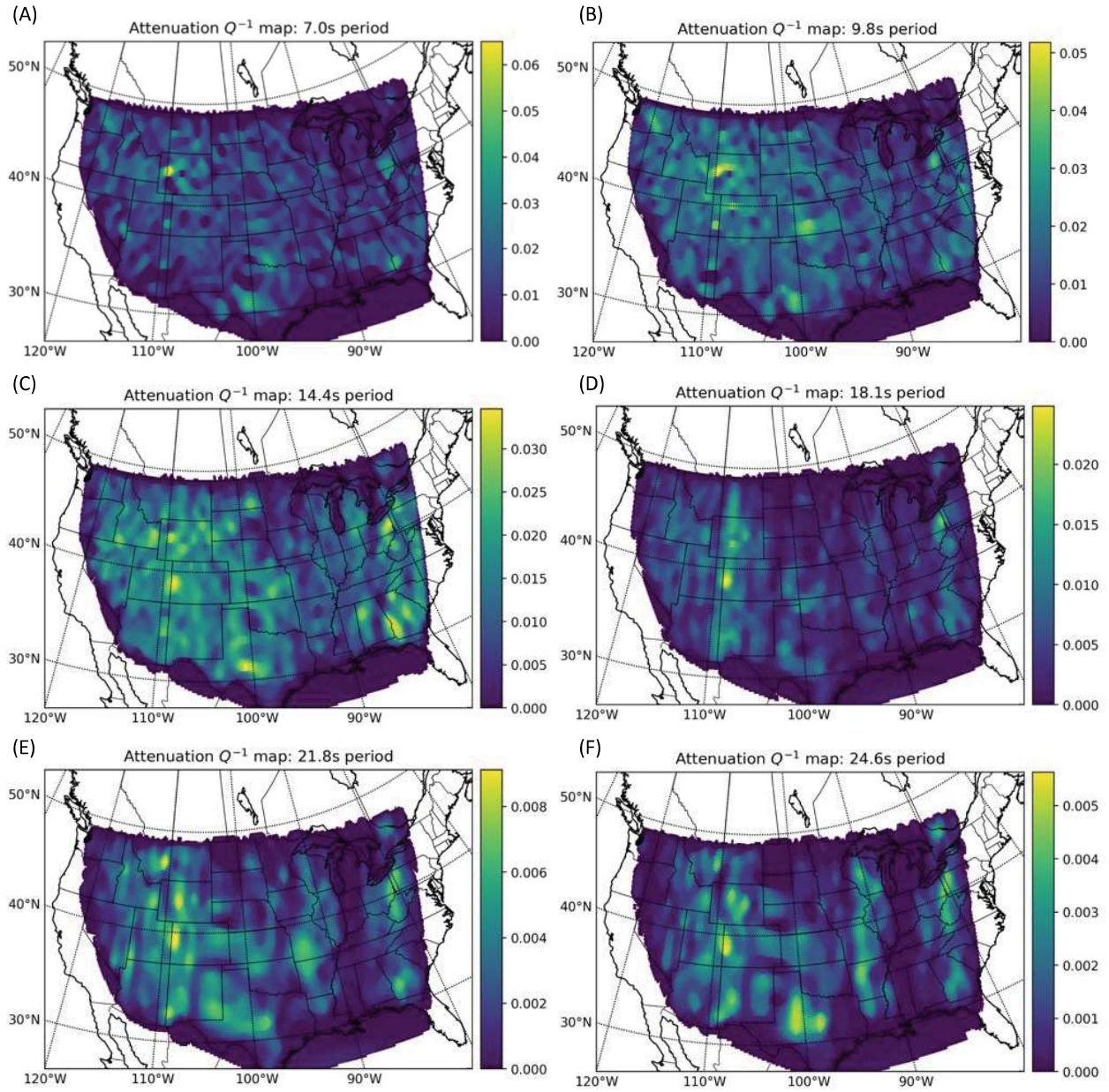


Figure 4: USArray attenuation $1/Q$ maps using 2D median filter with 126 km smoothing kernel size.

Based on the $1/Q$ values from linear triplets of stations, we estimate the $1/Q$ values for each line. We first project all stations within this line to a great circle, then we discretize the great circle arc between the first and the last stations using a grid spacing of 18 km. The $1/Q$ values in the linear grids are estimated for each line at each discrete frequency assuming straight ray paths based on the $1/Q$ measurements from the linear triplets of stations. Finally, we apply a 2D median smoothing filter with 126 km kernel size to the attenuation $1/Q$ map for each frequency. The resulting attenuation maps at six different periods are shown in Fig.4.

The Yellowstone caldera stands out at the periods 7.0 s and 9.8 s with strong attenuation of $1/Q \approx 0.065$, the location and strength of which is similar to the findings in previous studies [Lawrence and Prieto, 2011, Bowden et al., 2017]. It also appears on all other attenuation maps with stronger attenuation patterns than those in neighboring regions; however, the area of Yellowstone attenuation anomaly is three times larger in Lawrence and Prieto [2011], which may be related to overestimates of attenuation by their coherency method. The northern Colorado Plateau [Fenneman and Johnson, 1946] at the boundary between Utah and Colorado corresponds to strong attenuation of 0.03 at 14.4 s and also appears on the attenuation maps for periods between 18.1-24.6 s as a low- Q anomaly, which agrees with the study of [Levander et al., 2011] that the mantle asthenospheric upwelling is thought to uplift the Colorado Plateau. The Appalachian Mountains (low Q) show up on multiple attenuation maps for periods between 14.4-24.6 s. The Edwards Plateau in Texas also corresponds to attenuation $1/Q \approx 0.03$ at the period 14.4 s and appears on all other attenuation maps.

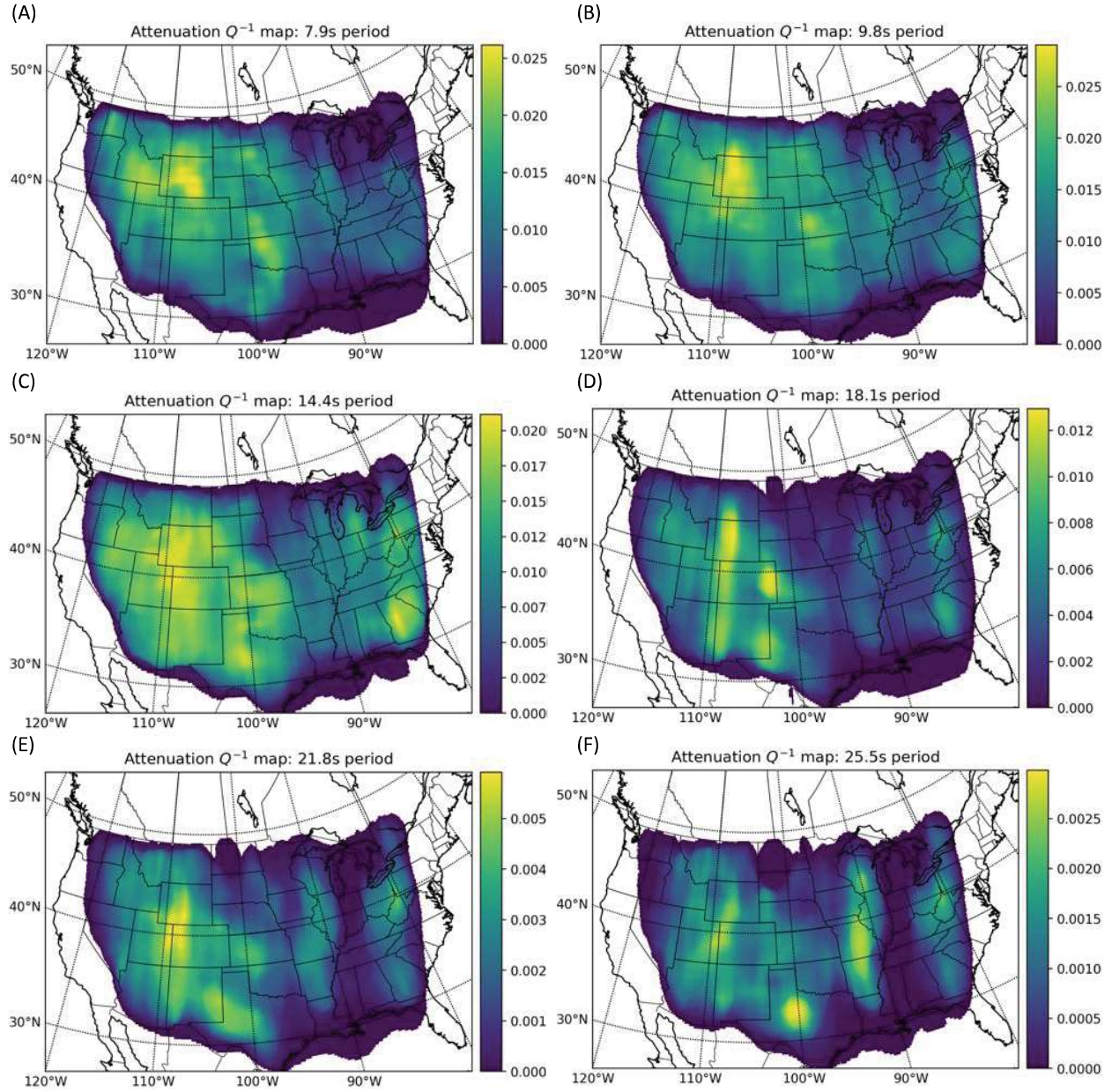


Figure 5: USArray smoothed attenuation $1/Q$ maps using 2D median filter with 450 km kernel size.

Applying a median smoothing filter with longer kernel size of 450 km, we obtain smoother attenuation $1/Q$ maps at six periods using USArray (Fig. 5). The strong attenuation around Yellowstone is broader at 7.9 s due to more spatial smoothing, but the Snake River Basin stands out to the west of Yellowstone. The Yellowstone hotspot appears on attenuation maps at all periods, although the patch with strongest

attenuation migrates to the south near the boundary of northern Colorado Plateau and Rocky Mountains. For periods between 14.4-25.5, the strong attenuation structure at northwestern Texas may correspond to the Grenville Front. The Appalachian Mountains also correlates with strong attenuation compared with the background in the eastern US for periods between 14.4-25.5 s. The general pattern for all inverted attenuation maps is that the western US is characterized by stronger attenuation than the eastern US. This dichotomy has been noted previously by many studies, but through our approach we should be able to quantify it, to regionalize it at a finer scale, and by using the ambient seismic field to do so even in areas without recent seismicity. Our attenuation model is freely available from the PIs on request.

References

- Daniel C Bowden, Victor C Tsai, and Fan-Chi Lin. Amplification and attenuation across usarray using ambient noise wavefront tracking. *Journal of Geophysical Research: Solid Earth*, 122(12):10–086, 2017.
- Nevin M Fenneman and DW Johnson. Physical divisions of the united states (map). *Reston, VA: US Geological Survey*, 1946.
- Jesse F Lawrence and Germán A Prieto. Attenuation tomography of the western united states from ambient seismic noise. *Journal of Geophysical Research: Solid Earth*, 116(B6), 2011.
- A Levander, B Schmandt, MS Miller, K Liu, KE Karlstrom, RS Crow, C-TA Lee, and ED Humphreys. Continuing colorado plateau uplift by delamination-style convective lithospheric downwelling. *Nature*, 472(7344):461, 2011.
- Xin Liu, Yehuda Ben-Zion, and Dimitri Zigone. Extracting seismic attenuation coefficients from cross-correlations of ambient noise at linear triplets of stations. *Geophysical Journal International*, 203(2): 1149–1163, 2015.
- Xin Liu, Yehuda Ben-Zion, and Dimitri Zigone. Frequency domain analysis of errors in cross-correlations of ambient seismic noise. *Geophysical Supplements to the Monthly Notices of the Royal Astronomical Society*, 207(3):1630–1652, 2016.
- Germán Prieto, Jesse FA Lawrence, and Gregory C Beroza. Anelastic earth structure from the coherency of the ambient seismic field. *Journal of Geophysical Research: Solid Earth*, 114(B07303), 2009.